Behaviour of Ti/Al/Ti/Au contacts to AlGaN/GaN heterostructures at low temperature

Francesca Adams[1],[*] , Saptarsi Ghosh[1] , Zhida Liang[1], Chen Chen[1] , Noppasorn Suphannarat[1], Menno J Kappers[1], David J Wallis[1,2] and Rachel A Oliver[1]

[1] Department of Materials Science and Metallurgy, University of Cambridge, 27 Charles Babbage Road, Cambridge CB3 0FS, United Kingdom
[2] Centre for High Frequency Engineering, University of Cardiff, 5 The Parade, Newport Road, Cardiff CF24 3AA, United Kingdom

E-mail: fa371@cam.ac.uk

CrossMark

Abstract

Ohmic contacts to wide bandgap nitrides have been realised, but little is known about their behaviour at low temperatures. To address this, an established Ti/Al/Ti/Au contact stack on AlGaN/GaN heterostructures has been characterised from 320 to 80 K. Two structures were investigated, with very similar ambient 2D electron gas transport characteristics despite their difference in AlGaN barrier thickness and composition. This allowed for direct comparison of contact behaviour across different heterostructures. Upon annealing at <800 °C for samples with 29 nm AlGaN barriers, contacts which had Ohmic characteristics at room temperature exhibited a gradual onset of Schottky behaviour as the measurement temperature was lowered. When non-Ohmic behaviour was observed, a combination of direct tunnelling, Fowler–Nordheim tunnelling and a thermally assisted Fowler–Nordheim mechanism is suggested to describe the carrier transport. In this case, annealing at 800 °C for 30 s proved sufficient to ensure Ohmic behaviour when tested from 320 to 80 K. For a heterostructure with 8 nm AlGaN, the required annealing temperature to maintain consistent Ohmic behaviour across the temperature range was reduced to 750 °C. From these observations, the determining factor for Ohmic behaviour is suggested to be the thickness of the AlGaN barrier–either as-grown, or the effective thickness following the formation of TiN protrusions into the AlGaN barrier during annealing. The understanding provided here allows tailoring of either the processing conditions or the heterostructure, and may aid with design of novel devices for low temperature operation.

Supplementary material for this article is available online

---

[*] Author to whom any correspondence should be addressed.

J. Phys. D: Appl. Phys. **58** (2025) 135117

F Adams *et al*

1. Introduction

AlGaN/GaN heterostructures form the basis of nitride high electron mobility transistors (HEMTs). The 2D electron gas (2DEG) that forms at the heterostructure interface has excellent transport properties, with typical mobilities of ~ 1500 cm^2 V^{-1} s^{-1} and sheet carrier densities in the order of 10^{13} cm^{-2} at room temperature [1]. As the temperature is decreased, the sheet carrier density remains high and the mobility improves by up to an order of magnitude [2, 3]. Such 2DEGs are exploited in the design of nitride HEMTs, wherein metallic contacts are deposited atop the heterostructure to allow connection to an external circuit and use as a transistor. The improved 2DEG properties at low temperatures are beneficial for a range of applications; for example, alongside superconducting components in high power electric motors for large-scale transport [4, 5]. Transistors with the capability to operate at the required cryogenic temperatures for effective superconductivity can help increase the overall efficiency and simplify the design of the system. Whilst AlGaN/GaN heterostructures form a promising basis for transistors for such applications due to the impressive performance of the 2DEG, reliable operation of the metallic contacts at low temperatures is also crucial.

Prior studies into contact behaviour have put significant emphasis on minimising the specific contact resistance, ρ_c, of Ohmic contacts. Whilst this is undeniably an important parameter, it alone cannot describe the full range of behaviour exhibited by the contacts [6]. Understanding the transport mechanisms behind the contact behaviour will facilitate better contacts without subjection to very high temperature anneals. In previous reports, the lowest values of ρ_c have been achieved following annealing at temperatures up to 950 °C [7–9]. However, not all structures are able to withstand these conditions. The most commercially viable normally-off HEMTs are fabricated with p-GaN gates [10–12], but structures containing p-GaN have been shown to degrade following exposure to high temperatures [11]. Rapid thermal annealing at elevated temperatures has also been suggested to increase the density of surface donor states, pinning the Fermi level [13], and a trend for worsening edge acuity of the contact metals at higher annealing temperatures has been identified [9, 14]. Furthermore, a recent study by Yu *et al* suggests the increased thermal budget from a high temperature annealing step could be detrimental to the 2DEG transport properties in AlGaN/AlN/GaN structures, lowering the mobility by exacerbating the alloy disorder scattering [15]. Therefore the emphasis for this work is not merely on reducing ρ_c, but on achieving reliable Ohmic contacts with relatively gentle annealing processes, and the dependence of this on the structural properties of the heterostructure.

The most common metallisation scheme used in the fabrication of Ohmic contacts to AlGaN/GaN heterostructures is a Ti/Al/*x*/Au stack. These metals have been carefully selected to enhance the Ohmic contact [16]: Ti reacts with nitrogen within the AlGaN barrier, forming TiN and leaving nitrogen vacancies, in a process controlled by the Al in the metal stack, which can also react with Ti. There are several metallic possibilities for the barrier layer '*x*' [17–20]; titanium is an established option that has been used here [14, 19–23]. The contacts have been fabricated with varying parameters, and their electrical characteristics probed. Several carrier transport mechanisms have previously been proposed in the context of Schottky contacts on AlGaN/GaN heterostructures in the reverse bias regime [24–30], and the applicability to this scenario has been assessed here. The majority of previous studies on Schottky contacts have focussed on temperatures upwards of 223 K [25, 31, 32], with those on Ohmic contacts focussing solely on reducing ρ_c. In this work, measurement temperatures varied from 320 down to 80 K, with the aim of providing practical engineering advice on the fabrication of contacts for this low temperature regime.

2. Methods

The AlGaN/GaN heterostructures used for this investigation were grown using MOVPE, with trimethyl gallium, trimethyl aluminium and ammonia precursors, on Si(111) substrates—a layer schematic is shown in figure 1(a). Two wafers were used in this investigation: wafer *A* has a nominally 29 nm thick Al$_{0.28}$Ga$_{0.72}$N barrier with room temperature mobility $\mu \approx 1850$ cm^2 V^{-1} s^{-1} and sheet carrier density $n_s \approx 1.1 \times 10^{13}$ cm^{-2}, and wafer *B* has a nominally 8 nm thick Al$_{0.39}$Ga$_{0.61}$N barrier with $\mu \approx 1800$ cm^2 V^{-1} s^{-1} and $n_s \approx 1.1 \times 10^{13}$ cm^{-2} at room temperature. These values were obtained from Hall measurements on samples patterned with Ohmic contacts in van der Pauw geometry. By adjusting both the AlGaN barrier thickness and composition, very similar transport characteristics are achieved, allowing direct comparison of carrier transport between wafers with different barrier properties. Both include a nominally 1 nm AlN exclusion layer to reduce penetration of the 2DEG into the barrier. The compositionally graded AlGaN buffer layer has been doped with iron using ferrocene to pin the Fermi level and reduce the effects of unintentional doping [33]. Both wafers were grown under identical conditions. For both, the barrier growth temperature was approximately 1025 °C, well above any temperatures the wafers were subjected to during the contact annealing procedure.

The selected metallisation scheme for this work is Ti/Al/Ti/Au, with intended thicknesses of 15/50/30/80 nm [19]. The geometry of the contacts is akin to a lateral diode, with a circular inner contact of diameter 766 μm surrounded by a larger annular outer contact at a separation of 400 μm. This is shown in figure 1(b), with an indication of how it was connected to the external circuit for testing. The outer contact is considered to be roughly Ohmic at all temperatures due to its large area. This geometry was achieved by employing standard photolithographic procedures, and annealing was then carried out in an RTP600S rapid thermal annealer. Annealing temperatures trialled were 700 °C, 750 °C and 800 °C, for 30 s, 60 s, 90 s and 120 s. Each combination of annealing temperature and time was performed on a different chip from the wafer.
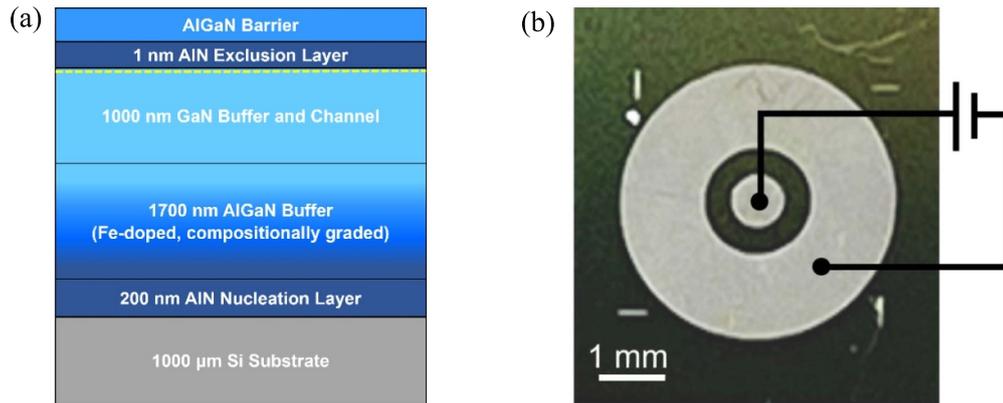
Figure 1. (a) Schematic of the AlGaN/GaN heterostructure. Wafer *A* has 29 nm of $Al_{0.28}Ga_{0.72}N$ and wafer *B* has 8 nm of $Al_{0.39}Ga_{0.61}N$. The dotted line represents the 2DEG. (b) Image of the deposited contact geometry, with a schematic of the external connections.

Electrical measurements were performed using an Ecopia HMS 5000 Hall effect measurement system, interfaced with a Keithley 2400 SourceMeter. In the Ecopia setup, the samples are immersed in liquid nitrogen and then heated in a controlled manner to 320 K. Measurements were taken every 40 K during this heating process, with a source voltage of -5 to $+5$ V and the current compliance set to 100 mA. Transmission electron microscopy (TEM) images and energy dispersive x-ray spectroscopy (EDX) were obtained with an FEI Tecnai Osiris equipped with a Super-X EDS detection system. Samples were prepared in a dual beam FEI Helios Nanolab focussed ion beam microscope (FIB).

3. Results and discussion

3.1. Effects of annealing temperature on current–voltage (I–V) characteristics

I–V curves were recorded between 80 and 320 K for wafers *A* and *B*, with contacts annealed at varying temperatures. Figure 2 shows these data for three contacted samples from wafer *A*: annealed at 700 °C, 750 °C and 800 °C, all for 30 s. Figure 2(a) shows non-linear characteristics, even at room temperature, with the extent of the non-linearity depending strongly on measurement temperature. This is similar to the turn-on characteristic seen for Schottky diodes, with the threshold voltage increasing as the temperature is lowered. At high applied voltages, the current flow increases at lower measurement temperatures, but the opposite trend is observed for the lower magnitude bias region. This gives rise to a 'crossover point', as shown on the plot for both the negative and positive bias quadrants. Figure 2(b) displays similar trends, but the crossover point has now shifted closer to the origin. In figure 2(c), the *I–V* plots are linear across the entire temperature range. There is zero threshold voltage, and these contacts can now be considered Ohmic. Contacts annealed at 800 °C for 60, 90 and 120 s also displayed Ohmic behaviour, but annealing at 700 °C for 120 s was insufficient to ensure Ohmic

behaviour at low temperatures. Henceforth, samples annealed at 700 °C, 750 °C and 800 °C for 30 s will be the focus, to explore the (seemingly greater) dependence on annealing temperature as opposed to time.

The overall electrical behaviour is a combination of any external metallic connections (taken to have very low resistance), the contact resistance and the resistance of the 2DEG. This total resistance is given by the inverse gradient of the *I–V* plots. At biases of greater magnitude than the crossover point in figures 2(a) and (b) and all biases in figure 2(c), the total resistance can be seen decreasing as the temperature is lowered. This is the expected trend for AlGaN/GaN heterostructures with Ohmic contacts, as confirmed by variable temperature Hall measurements on these wafers. At higher bias, the contact resistances must therefore be lower than that of the 2DEG, as the behaviour of the latter appears to dominate the temperature dependence of the electrical characteristics beyond the crossover point. At smaller magnitude biases in figures 2(a) and (b), the contacts appear to provide the dominant contribution. The crossover point marks the boundary between these two regimes.

Similar characteristics for wafer *B* are shown in figure 3. Whilst there is some non-linearity illustrated in figure 3(a), annealed at 700 °C for 30 s, it is significantly smaller in extent than that seen in figure 2(a) for wafer *A*. Figures 3(b) and (c) show complete linearity within the accuracy of our measurement. This suggests the barrier characteristics strongly influence the electrical behaviour, which will be explored in greater detail in section 3.

For subsequent analysis, the reverse bias regime has been selected, allowing equivalent comparisons to reverse bias leakage in Schottky diodes [24–30]. This corresponds to the inner contact being negatively biased and the outer contact being positively biased. Despite the inner and outer contacts being fabricated identically, such analysis is assumed applicable due to the much larger area of the outer contact.

Focussing on the non-Ohmic regime shown in figures 2(a) and (b), the *I–V* characteristics for the reverse bias region
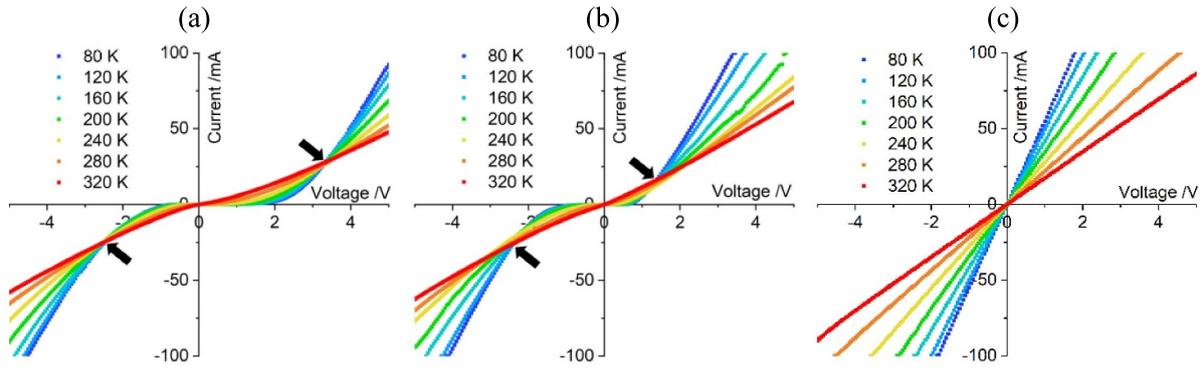
Figure 2. Current–voltage characteristics for three samples from wafer *A*, annealed at (a) 700 °C, (b) 750 °C and (c) 800 °C, all for 30 s. Crossover points are marked with black arrows.
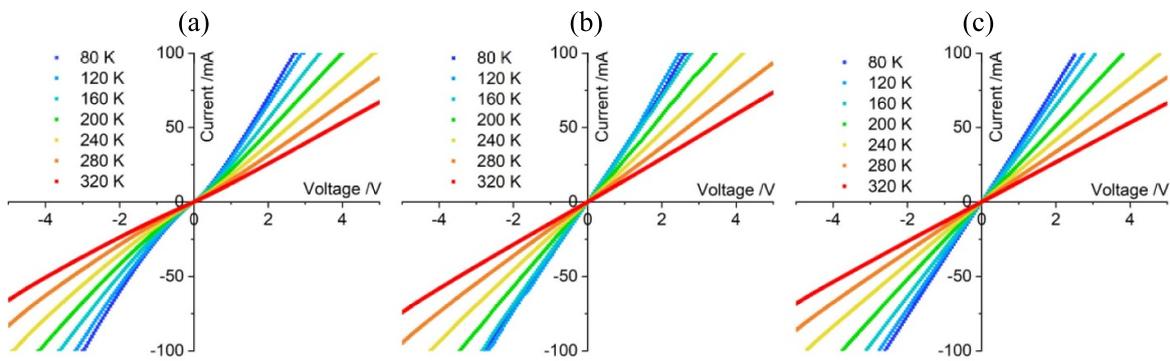
Figure 3. Current–voltage characteristics for three samples from wafer *B*, annealed at (a) 700 °C, (b) 750 °C and (c) 800 °C, all for 30 s.
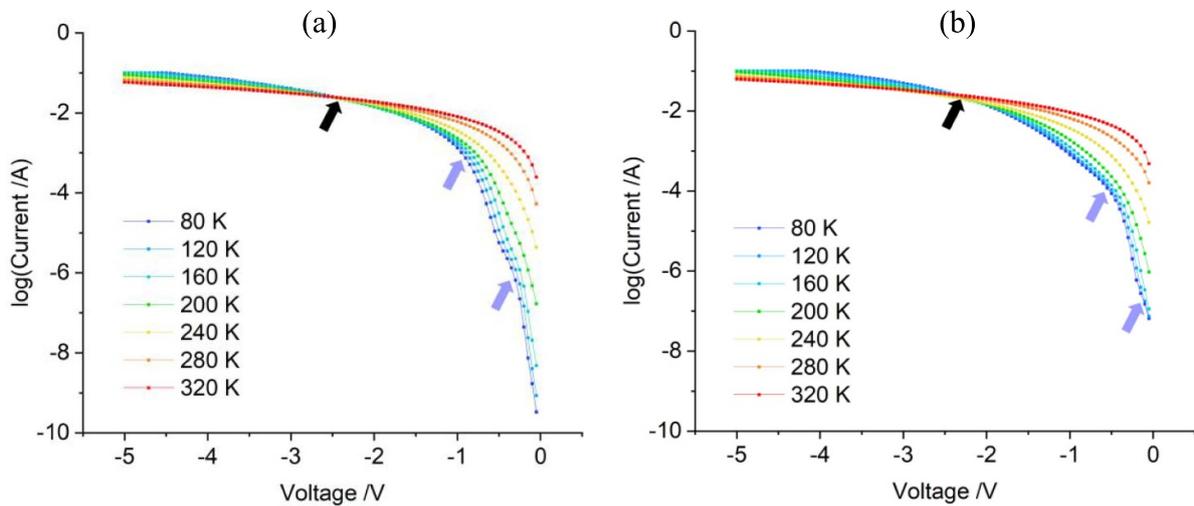
Figure 4. Plots of log(current) vs voltage for the two samples from wafer *A* showing non-Ohmic behaviour, annealed at (a) 700 °C and (b) 750 °C for 30 s. Black arrows indicate the crossover points, and shoulders in the data, indicating that different carrier transport mechanisms are applicable in different temperature and bias regimes, are marked by purple arrows.

of these samples are shown on a log scale in figure 4. The crossover points discussed above have again been labelled, and further analysis will consider biases of lower magnitude than this, where the contacts are suggested to be the primary contribution to the observed trends. Inspection of figure 4(a)

up to this point reveals the currents increase with the magnitude of the applied bias and with increasing measurement temperatures, with the impact of temperature being most pronounced under low magnitude bias. There are also 'shoulders' in the plots, which are particularly prevalent at

lower temperatures. Figure 4(b) shows similar trends, but generally higher currents. The positions of the shoulders have also shifted to lower magnitude biases. The presence of these shoulders suggests there is no single carrier transport mechanism that dominates over the entire voltage range, particularly at lower temperatures, but rather a combination of mechanisms is acting. Possible mechanisms will be considered in subsequent sections, with a tentative proposition for dominant (but not sole) mechanisms in different regimes across the voltage and temperature range being discussed in section 4. The samples show some leakage, but this is not uncommon for Schottky diodes on GaN [34, 35]. The following section explores the carrier transport.

3.2. Modelling non-Ohmic behaviour

In ideal Ohmic contacts, electron transport does not appear hindered upon inspection of the *I*–*V* plots. In reality, there may be a barrier present, yet it is small enough for carriers to tunnel through without observably affecting the data. This tunnelling process is, in the ideal case, independent of temperature, with the only source of temperature dependence for the *I*–*V* curves in figure 2(c) then being the expected semiconductor properties. In this regime, the resistance decreases as the temperature is lowered, as discussed. However, where an opposite temperature dependence is observed, as for the non-Ohmic samples here, this implies there is a further, temperature-dependent mechanism at play, affecting the transport of carriers into the semiconductor. *A* number of mechanisms have been suggested to describe reverse leakage carrier transport in AlGaN/GaN Schottky diodes [25, 31, 32, 36, 37]. These include trap-assisted tunnelling, Frenkel–Poole emission and Fowler–Nordheim tunnelling. These studies often suggest involvement of multiple mechanisms acting simultaneously, tending also to investigate the higher temperature rather than low temperature regimes.

Analyses in this section will focus on the sample annealed at 700 °C for 30 s, as this displayed the greatest degree of non-linearity in its *I*–*V* characteristics—other samples will be explained with reference to the behaviour of this sample. Fowler–Nordheim tunnelling considers tunnelling through a triangular energy barrier, giving a current, *I*, that depends on field, *E*, as described by equation (1) [25]:

$$I_{\text{FN}} = AE^2 \exp\left(-\frac{B}{E}\right), \tag{1}$$

where *A* and *B* are constants. Therefore a straight line on a plot of $\ln\left(\frac{I_{\text{FN}}}{E^2}\right)$ against $\frac{1}{E}$ would indicate that Fowler–Nordheim tunnelling is dominant. Figure 5(a) shows a plot for this sample, over the entire studied temperature range, at reverse biases up to the crossover point. *A* temperature dependence can be seen, with the measurement temperature having a bigger impact at lower magnitude biases. All the plots have a negative gradient, but it is not constant over the entire voltage range.

Figure 5(b) shows a zoom of figure 5(a), highlighting the region with higher applied field. Linear fits within this regime

are shown. The extent to which Fowler–Nordheim tunnelling appears applicable changes depending on the measurement temperature. From 80 to 160 K, the linear fit seems appropriate at applied negative bias greater than roughly 1 V in magnitude ($\frac{1}{E} < 0.0085$ m MV^{-1}). There is also very little temperature dependence in this regime. Relating this back to figure 4(a), the top shoulder occurs at approximately −1 V, appearing to correlate to the onset of linear behaviour in figure 5. At temperatures above 160 K, the linear fits for each temperature seem suitable across a wider range of applied field, but there is greater variation with measurement temperature. Referring back to equation (1), Fowler–Nordheim tunnelling alone does not exhibit a temperature dependence.

With this in mind, equation (1) can be modified with an Arrhenius multiplier to acknowledge the contribution of a thermally activated process to the overall mechanism of carrier transport. The activation energy for this process is denoted by E_{A}:

$$I_{\text{FN}} = AE^2 \exp\left(-\frac{B}{E}\right) \exp\left(-\frac{qE_{\text{A}}}{kT}\right). \tag{2}$$

As an example, an Arrhenius plot for this sample is shown in figure 5(c), at an applied negative bias of 1.5 V. This reveals two distinct regimes. At temperatures from 80 K to 160 K, the gradient is very shallow. In this regime, the non-thermally dependent Fowler–Nordheim tunnelling appears to be an applicable mechanism of carrier transport. At temperatures exceeding 160 K, there is a second straight line of steeper gradient. From this, an activation energy of 0.025 eV can be calculated. Physically, this is suggested to describe a thermally assisted Fowler–Nordheim tunnelling regime, wherein electrons are thermally promoted to a level from which Fowler–Nordheim tunnelling is possible. This is well supported by the fact that the calculated activation energy, 0.025 eV, is equal to $\frac{3}{2}kT$ at 200 K.

The question then remains as to the most dominant carrier transport mechanism at temperatures of 160 K and below and applied negative biases smaller than 1 V in magnitude. Here, the data in figure 5(b) begin to deviate from the linear fit, indicating Fowler–Nordheim tunnelling is no longer suitable. Equation (3) relates to a direct tunnelling mechanism, wherein tunnelling through the barrier occurs regardless of the barrier shape [38]. For this dataset, the exponential factor *C* will not change between samples or temperatures:

$$\ln(I) = \ln(V) - C. \tag{3}$$

Figure 5(d) shows the ln(*I*) vs ln(*V*) plot for the low temperature, low applied field regime. The linear fits appear roughly applicable within a limited range (ln(*E*) < 18.35), suggesting direct tunnelling may be the dominant (but perhaps not sole) mechanism at these low applied fields. Diagrams representing the transport mechanisms discussed will be presented and explained in section 4.

This analysis so far has referred to the sample annealed at 700 °C for 30 s, but the analysis proves very similar for
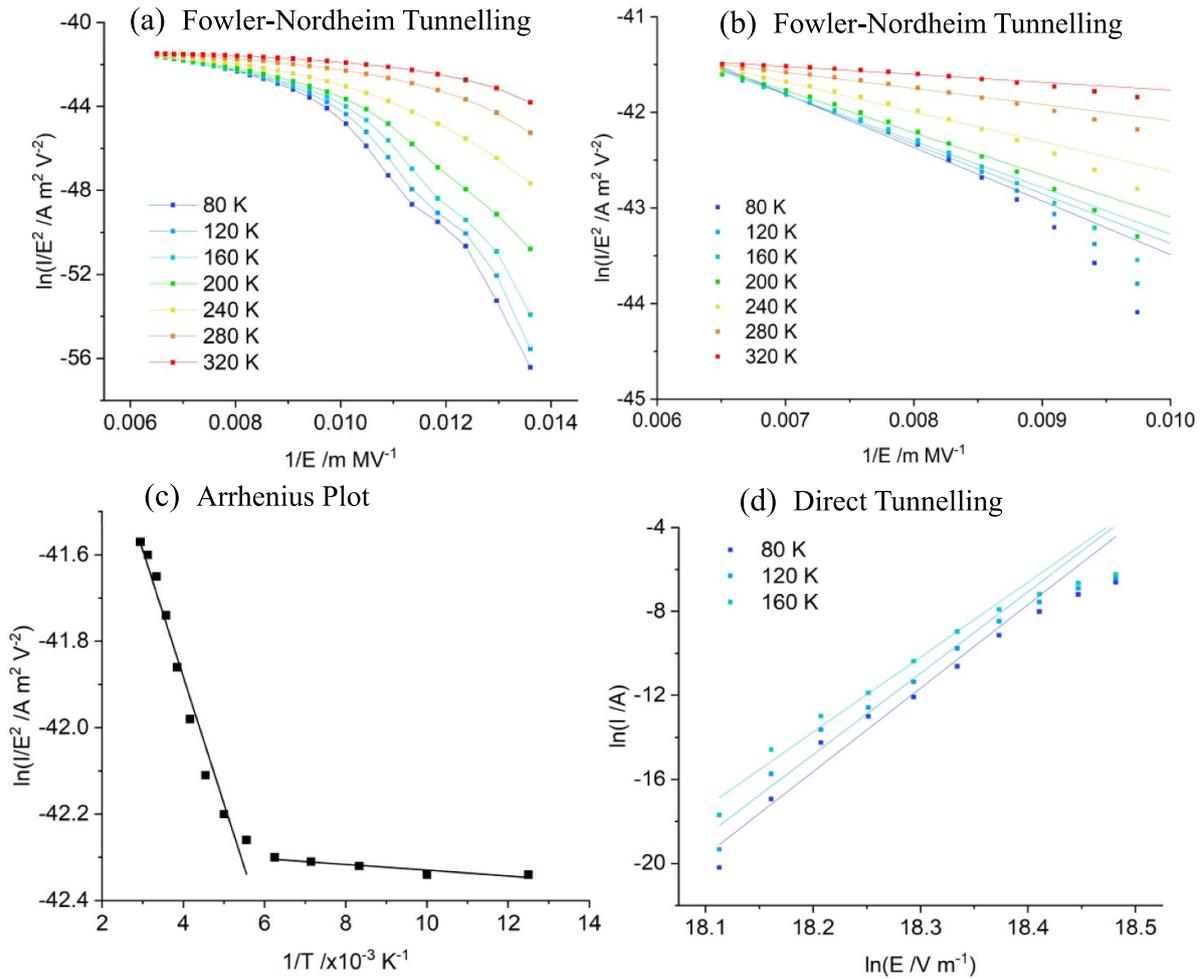
Figure 5. (a) Fowler–Nordheim tunnelling plot for the sample from wafer *A* annealed at 700 °C for 30 s. (b) Zoom of this plot with initial linear fits shown, indicating the applicable regime for this mechanism. (c) Arrhenius-style plot illustrating different regimes of temperature dependence. (d) Direct tunnelling plot, with linear fits indicating the region where this mechanism is valid.

other samples. For example, reproducing this modelling for the sample annealed at 750 °C for 30 s shows very similar trends; Fowler–Nordheim tunnelling, its thermally assisted variant, and direct tunnelling all have apparent regions of being the most dominant transport mechanism. The main variation between samples is the onset of the different mechanisms. The position where direct tunnelling appears more applicable than Fowler–Nordheim tunnelling occurs at a smaller magnitude bias for the sample annealed at 750 °C compared to 700 °C. This is consistent with the positions of the shoulders in figure 4(b) shifting to lower absolute biases than in figure 4(a).

Considering alternative mechanisms, an Arrhenius temperature dependence has also been shown to correlate to both Frenkel–Poole emission [26] and trap-assisted tunnelling [27]. However, neither of these mechanisms appear to fit the results obtained here as effectively (see supplementary information). Greco *et al* [32] present an Arrhenius dependence for a 2D variable-range hopping mechanism, but their calculated activation energy is an order of magnitude larger than the value obtained here, suggesting this mechanism is not suitable either in this case.

3.3. TEM of metal/AlGaN interface

To correlate the observed electrical behaviour with microstructural characteristics, the samples have been imaged in cross section using TEM. The images obtained illustrate the formation of an extra layer between the AlGaN surface and the deposited metal, confirmed by EDX to be TiN—see figure 6. This layer is approximately 1 to 2 nm wide. For each sample, the AlGaN barrier thickness after annealing was measured by counting lattice fringes on high resolution images (images in supplementary information). Within each image, the thickness was taken as the mean over five positions. For the images obtained, no significant difference in AlGaN barrier thickness following annealing at different temperatures was observed. However, some changes upon annealing at higher temperatures were seen when observing a broader area of the samples. Figure 7 shows a TEM image from the wafer *A* sample annealed at 800 °C, the hottest temperature trialled in this work, for 30 s. This sample showed Ohmic behaviour. A protrusion, confirmed with EDX to be TiN, was seen at the metal-AlGaN interface, but no such protrusions were identified within the imaged regions of the other samples.
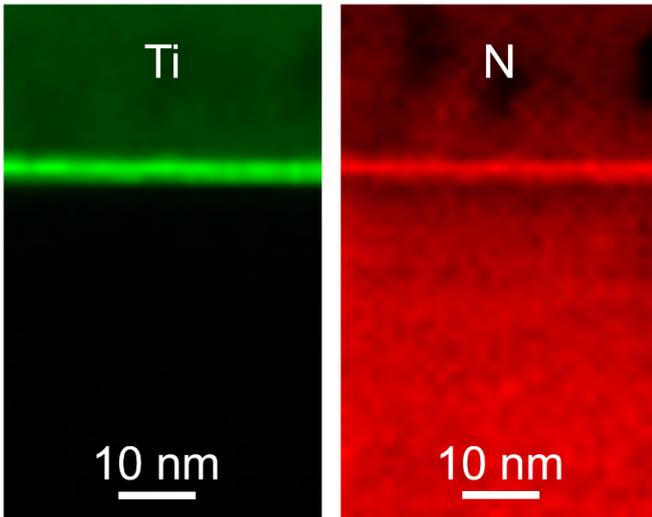
Figure 6. EDX scans showing a layer rich in Ti and N at the interface of metal (above) and AlGaN (below). This sample was annealed at 700 °C for 30 s.
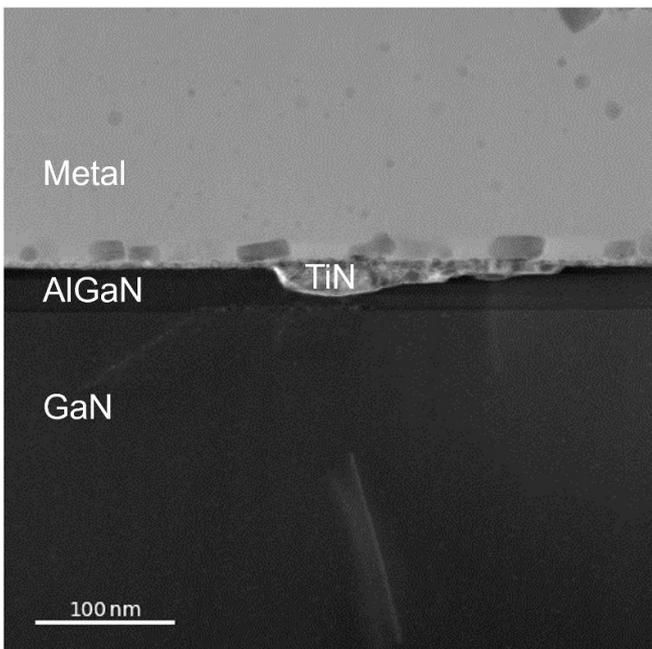
Figure 7. Cross-sectional TEM image of wafer *A*, showing the protrusion of the TiN layer into the AlGaN barrier, for the sample annealed at 800 °C for 30 s.

The interfacial TiN is formed during the annealing step, consuming some of the AlGaN barrier in the process. As this reaction proceeds, nitrogen is drawn from the AlGaN barrier, resulting in the formation of nitrogen vacancies [16, 39, 40]. These are negatively charged, so increase the local carrier concentration. Formation of TiN was confirmed at all annealing temperatures, but there were no significant differences between the thicknesses of the interfacial layer following the varying annealing steps. For wafer *A*, with its thick AlGaN barrier as-grown, protrusions such as that observed

in the sample annealed at 800 °C are suggested to be the determining factor for Ohmic behaviour at all measurement temperatures. Such protrusions have previously been suggested to assist with Ohmic contact formation, by shortening the tunnelling distance between the metal and 2DEG within the heterostructure [41] or even consuming the entire AlGaN barrier so as to directly contact the 2DEG [19, 42, 43]. They have been linked to the presence of threading dislocations in the AlGaN/GaN. Notably, the protrusion here does not consume the entire AlGaN barrier—roughly 8 nm remains—but this contact still retains Ohmic behaviour to 80 K. Assuming this protrusion is a significant aid to Ohmic contact formation, this demonstrates that total barrier consumption is not essential to ensure Ohmic behaviour—there may instead be a minimum AlGaN thickness through which tunnelling is trivial. This suggestion is supported by experiments on wafer *B*. With a nominal 8 nm barrier as-grown, Ohmic contacts at all measurement temperatures were formed after annealing at 750 °C for 30 s, as shown in figure 3(b). The fact that there is still a minimum annealing temperature required to achieve Ohmic behaviour at all measurement temperatures for wafer *B* indicates that, regardless of protrusion formation, the TiN interfacial layer formed during the annealing process is critical for ensuring Ohmic contacts.

3.4. Discussion and proposed transport scheme

Collating all the above observations, conduction band diagrams for the tentatively proposed carrier transport mechanisms for different electric field and temperature regimes are shown in figure 8. The diagrams also indicate additional electron states that are available at energies greater than the Fermi level, hypothesised to be surface trap states that have been enhanced by the thermal annealing process. Traps are known to be present at the AlGaN surface of AlGaN/GaN heterostructures [44], and the process of annealing may increase the number of surface trap states [45]. The exact nature of these trap states is difficult to determine, but their presence and related energy levels could be confirmed by deep-level transient spectroscopy [46] or current transient spectroscopy [47], which is beyond the scope of this report.

- Figure 8(a) illustrates direct tunnelling, wherein the electron must tunnel through the entire width of the barrier, regardless of its shape.
- Figure 8(b) shows Fowler–Nordheim tunnelling. Under this applied bias, the energy band skews, to the extent that the Fermi level in the semiconductor drops below that in the metal. This results in the triangular energy barrier shown.
- Figure 8(c) represents a thermally assisted Fowler–Nordheim scheme. The electrons within the metal can now be thermally promoted to the higher available states prior to tunnelling. This promotion leads to a smaller required tunnelling distance, at which point the thermal promotion effectively becomes the rate-limiting step to carrier transport.
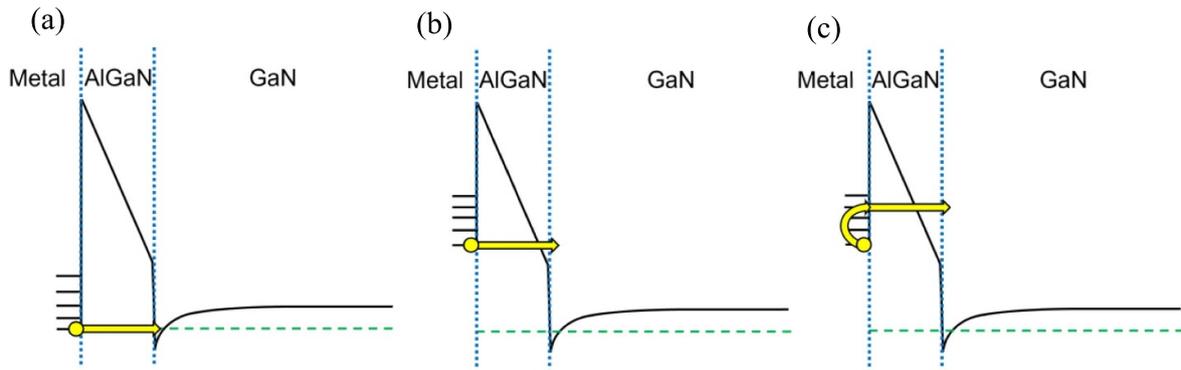
Figure 8. Conduction band diagrams for the proposed transport mechanisms, illustrating (a) direct tunnelling, suggested at temperatures up to 160 K and low magnitude applied bias, (b) Fowler–Nordheim tunnelling, suggested at the same low temperatures but greater magnitude applied bias, and (c) thermally assisted Fowler–Nordheim tunnelling, suggested for temperatures greater than 160 K. The green dashed line represents the Fermi level.

These three suggested mechanisms together provide a possible description of the dominant mechanisms of carrier transport across the studied range of biases and temperatures, although other mechanisms may also play a role. Direct tunnelling is tentatively hypothesised to be the primary transport mechanism at temperatures from 80 to 160 K under applied reverse bias of low magnitude ($<$1 V). With greater magnitude reverse bias but still low temperatures, so the higher energy states are unattainable, Fowler–Nordheim tunnelling seems applicable. At increased temperatures, the higher energy states can be reached by thermal promotion, and it seems the Fowler–Nordheim tunnelling can be modified with an Arrhenius-like thermal dependence.

The above is applicable to non-Ohmic contacts, with the analysis being carried out on samples from wafer *A* following annealing at 700 °C and 750 °C for 30 s. TEM analysis confirmed the formation of TiN in all samples, but protrusion formation was only seen following annealing at 800 °C for 30 s, which resulted in Ohmic behaviour at all measurement temperatures down to 80 K. The remaining barrier under this protrusion was roughly 8 nm, equal to the initial barrier thickness of wafer *B*. For this latter wafer, no protrusions were observed, but the samples were Ohmic down to 80 K. This implies the key factor is the remaining thickness of AlGaN to tunnel through. Contact pads for circular transmission line measurement studies [48] were fabricated on wafer *B*, with inner diameter 200 μm and separations ranging from 20 to 100 μm, and annealed at 800 °C for 60 s. From these, contact resistances were calculated as (5.6 ± 0.9) Ω mm at room temperature and (4.7 ± 0.9) Ω mm at 80 K, similar values to those reported by Fay *et al* [19]. The tendency for non-Ohmic behaviour to become apparent at cryogenic temperatures indicates that measuring electrical properties at low temperatures may be a useful approach to ensure completeness of future contact studies.

These findings also highlight the need to tailor the fabrication process for the sample in question—heterostructures with different barrier properties will have different processing requirements to ensure Ohmic contacts. The area of the contact should also be considered; for very small contact areas, the likelihood of a protrusion being present would be lower given a fixed number density of protrusions. Conversely, more protrusions would be expected for contacts of much larger area. This supports the treatment of the larger outer contact as Ohmic in our analysis.

The ability to tailor the heterostructure and subsequent processing in this manner can prove beneficial in its own right, giving two methods—adapting the heterostructure itself (specifically the AlGaN barrier properties) or the contact fabrication process—of achieving the desired electrical behaviour. For example, if thermal budget is a concern, a thinner AlGaN barrier facilitates Ohmic contact formation with lower temperature annealing steps. On the other hand, if a thick AlGaN barrier is required, Ohmic contacts are still achievable by increasing the annealing temperature. The intended device application is also a consideration—for RF applications thinner barriers are generally preferred, whereas power devices may use thicker AlGaN barriers. Increasingly, the use of a Schottky drain contact has been reported to give higher breakdown voltage and lower leakage current in AlGaN/GaN HEMTs [23, 49–52]. The ability to control the degree of rectifying behaviour through adapting the fabrication process could improve their functionality, when compared to using conventional high work function metal contacts such as Ni/Au [53, 54]. An alternative approach to achieving Ohmic behaviour at low annealing temperatures is the use of gold-free contact metallisations, such as Ta/Al-based contacts. These enable Ohmic contact formation at even lower annealing temperatures (around 600 °C), but may require an extra step of recess etching the AlGaN barrier [55, 56]. Additionally, the behaviour of these contacts at low temperatures has not been explored.

4. Conclusion

The effects of varying annealing conditions on the low temperature behaviour of Ti/Al/Ti/Au contacts to AlGaN/GaN heterostructures were investigated. Two wafers were tested, which possessed very similar ambient Hall effect characteristics despite their different AlGaN barrier properties. For the

heterostructure with a 29 nm AlGaN barrier, contacts annealed at 700 °C and 750 °C for 30 s were found to display an onset of Schottky behaviour as the measurement temperature was lowered from 320 K. Analysis of the contact characteristics, in the regime where the contacts dominated the overall behaviour, showed a combination of carrier transport mechanisms. At temperatures up to 160 K and under low magnitude reverse bias, direct tunnelling has been tentatively suggested to dominate, although it may not be the sole mechanism operational even under these conditions. As the magnitude of the applied bias increases, Fowler–Nordheim tunnelling seems more applicable, and at higher temperatures thermal promotion to trap states was suggested to occur prior to the proposed Fowler–Nordheim tunnelling, reducing the effective tunnelling distance. TEM images, coupled with EDX analysis, confirmed the formation of a TiN layer at the metal-semiconductor interface. Protrusions of this layer into the AlGaN barrier were identified as the determining factor for Ohmic behaviour at all temperatures. It is not necessary for these protrusions to completely consume the AlGaN barrier and contact the 2DEG; a shortening of the tunnelling distance through partial barrier consumption proved sufficient. In this case, annealing at 800 °C for 30 s enabled the formation of local protrusions which consumed all but ∼8 nm of the AlGaN barrier. Correspondingly, contacts to a wafer with nominally 8 nm of AlGaN as-grown presented Ohmic characteristics at 80 K after annealing at 750 °C for 30 s—no protrusions were observed in this case. This demonstrates the ability to fabricate low temperature Ohmic contacts to AlGaN/GaN heterostructures, even with thick AlGaN barrier layers, without the need to anneal at temperatures exceeding 800 °C.

Data availability statement

The data that support the findings of this study are openly available at the following URL/DOI: https://doi.org/10.17863/CAM.115326.

Acknowledgments

ORCID iDs

Francesca Adams https://orcid.org/0009-0008-2033-2121
Saptarsi Ghosh https://orcid.org/0000-0003-1685-6228
Chen Chen https://orcid.org/0000-0001-9931-2650
Rachel A Oliver https://orcid.org/0000-0003-0029-3993

References

[1] Mishra U K, Parikh P and Wu Y-F 2002 AlGaN/GaN HEMTs-an overview of device operation and applications *Proc. IEEE* **90** 1022–31
[2] Dogmus E *et al* 2016 InAlGaN/GaN HEMTs at cryogenic temperatures *Electronics* **5** 31
[3] Tülek R, Ilgaz A, Gökden S, Teke A, Öztürk M K, Kasap M, Özçelik S, Arslan E and Özbay E 2009 Comparison of the transport properties of high quality AlGaN/AlN/GaN and AlInN/AlN/GaN two-dimensional electron gas heterostructures *J. Appl. Phys.* **105** 013707
[4] Dezhin D S and Dezhina I N 2022 Development of the future aircraft propulsion system based on HTS electrical equipment with liquid hydrogen cooling *IEEE Trans. Appl. Supercond.* **32** 1–5
[5] Haran K S *et al* 2017 High power density superconducting rotating machines—development status and technology roadmap *Supercond. Sci. Technol.* **30** 123002
[6] Pelto C M, Austin Chang Y, Chen Y and Stanley Williams R 2001 Issues concerning the preparation of ohmic contacts to n-GaN *Solid State Electron.* **45** 1597–605
[7] Jacobs B, Kramer M C J C M, Geluk E J and Karouta F 2002 Optimisation of the Ti/Al/Ni/Au contact on AlGaN/GaN FET structures *J. Cryst. Growth* **241** 15–18
[8] Wang L, Mohammed F M and Adesida I 2008 Formation mechanism of Ohmic contacts on AlGaN/GaN heterostructure: electrical and microstructural characterizations *J. Appl. Phys.* **103** 093516
[9] Mohammed F M, Wang L, Adesida I and Piner E 2006 The role of barrier layer on Ohmic performance of Ti/Al-based contact metallizations on AlGaN/GaN heterostructures *J. Appl. Phys.* **100** 023708
[10] Jones E A, Wang F F and Costinett D 2016 Review of commercial GaN power devices and GaN-based converter design challenges *IEEE J. Emerg. Sel. Top. Power Electron.* **4** 707–19
[11] Greco G, Iucolano F and Roccaforte F 2018 Review of technology for normally-off HEMTs with p-GaN gate *Mater. Sci. Semicond. Process.* **78** 96–106
[12] Wadsworth A, Thrimawithana D J, Zhao L, Neuburger M, Oliver R A and Wallis D J 2023 GaN-based cryogenic temperature power electronics for superconducting motors in cryo-electric aircraft *Supercond. Sci. Technol.* **36** 094002
[13] Higashiwaki M, Chowdhury S, Miao M-S, Swenson B L, de Walle Cg V and Mishra U K 2010 Distribution of donor states on etched surface of AlGaN/GaN heterostructures *J. Appl. Phys.* **108** 063719
[14] Yanxu Z, Weiwei C, Yuyu F, Ye D and Chen X 2014 Effects of rapid thermal annealing on ohmic contact of AlGaN/GaN HEMTs *J. Semicond.* **35** 026004
[15] Yu H, Parvais B, Zhao M, Rodriguez R, Peralagu U, Alian A and Collaert N 2022 Thermal budget increased alloy disorder scattering of 2DEG in III–N heterostructures *Appl. Phys. Lett.* **120** 213504
[16] Van Daele B, Van Tendeloo G, Ruythooren W, Derluyn J, Leys M R and Germain M 2005 The role of Al on Ohmic contact formation on n-type GaN and AlGaN/GaN *Appl. Phys. Lett.* **87** 061905
[17] Benakaprasad B, Eblabla A M, Li X, Crawford K G and Elgaid K 2020 Optimization of ohmic contact for AlGaN/GaN HEMT on low-resistivity silicon *IEEE Trans. Electron Devices* **67** 863–8
[18] Fay M W, Han Y, Brown P D, Harrison I, Hilton K P, Munday A, Wallis D, Balmer R S, Uren M J and Martin T 2008 Structural and electrical characterization of AuPtAlTi ohmic contacts to AlGaN/GaN with varying annealing temperature and Al content *J. Appl. Phys.* **103** 074501

[19] Fay M W, Moldovan G, Brown P D, Harrison I, Birbeck J C, Hughes B T, Uren M J and Martin T 2002 Structural and electrical characterization of AuTiAlTi/AlGaN/GaN ohmic contacts *J. Appl. Phys.* **92** 94–100

[20] Wang C and Kim N-Y 2012 Electrical characterization and nanoscale surface morphology of optimized Ti/Al/Ta/Au ohmic contact for AlGaN/GaN HEMT *Nanoscale Res. Lett.* **7** 107

[21] Bardwell J A, Sproule G I, Liu Y, Tang H, Webb J B, Fraser J and Marshall P 2002 Comparison of two different Ti/Al/Ti/Au ohmic metallization schemes for AlGaN/GaN *J. Vac. Sci. Technol.* B **20** 1444–7

[22] Vertiatchikh A, Kaminsky E, Teetsov J and Robinson K 2006 Structural properties of alloyed Ti/Al/Ti/Au and Ti/Al/Mo/Au ohmic contacts to AlGaN/GaN *Solid State Electron.* **50** 1425–9

[23] Lian Y-W, Lin Y-S, Lu H-C, Huang Y-C and Hsu S S H 2012 AlGaN/GaN HEMTs on silicon with hybrid schottky–ohmic drain for high breakdown voltage and low leakage current *IEEE Electron Device Lett.* **33** 973–5

[24] Fu K *et al* 2020 Reverse leakage analysis for as-grown and regrown vertical GaN-on-GaN schottky barrier diodes *IEEE J. Electron Devices Soc.* **8** 74–83

[25] Turuvekere S, Karumuri N, Rahman A A, Bhattacharya A, DasGupta A and DasGupta N 2013 Gate leakage mechanisms in AlGaN/GaN and AlInN/GaN HEMTs: comparison and modeling *IEEE Trans. Electron Devices* **60** 3157–65

[26] Jin Ha W, Chhajed S, Jae Oh S, Hwang S, Kyu Kim J, Lee J-H and Kim K-S 2012 Analysis of the reverse leakage current in AlGaN/GaN schottky barrier diodes treated with fluorine plasma *Appl. Phys. Lett.* **100** 132104

[27] Yao Y *et al* 2014 Current transport mechanism of AlGaN/GaN schottky barrier diode with fully recessed Schottky anode *Jpn. J. Appl. Phys.* **54** 011001

[28] Hsu J W P, Manfra M J, Lang D V, Richter S, Chu S N G, Sergent A M, Kleiman R N, Pfeiffer L N and Molnar R J 2001 Inhomogeneous spatial distribution of reverse bias leakage in GaN schottky diodes *Appl. Phys. Lett.* **78** 1685–7

[29] Meneghini M, Bertin M, Stocco A, Dal Santo G, Marcon D, Malinowski P E, Chini A, Meneghesso G and Zanoni E 2013 Degradation of AlGaN/GaN schottky diodes on silicon: role of defects at the AlGaN/GaN interface *Appl. Phys. Lett.* **102** 163501

[30] Lim W, Jeong J-H, Lee J-H, Hur S-B, Ryu J-K, Kim K-S, Kim T-H, Song S Y, Yang J-I and Pearton S J 2010 Temperature dependence of current-voltage characteristics of Ni–AlGaN/GaN schottky diodes *Appl. Phys. Lett.* **97** 242103

[31] Turuvekere S, Rawal D S, DasGupta A and DasGupta N 2014 Evidence of fowler–nordheim tunneling in gate leakage current of AlGaN/GaN HEMTs at room temperature *IEEE Trans. Electron Devices* **61** 4291–4

[32] Greco G, Fiorenza P, Spera M, Giannazzo F and Roccaforte F 2021 Forward and reverse current transport mechanisms in tungsten carbide schottky contacts on AlGaN/GaN heterostructures *J. Appl. Phys.* **129** 234501

[33] Cordier Y, Azize M, Baron N, Chenot S, Tottereau O and Massies J 2007 AlGaN/GaN HEMTs regrown by MBE on epi-ready semi-insulating GaN-on-sapphire with inhibited interface contamination *J. Cryst. Growth* **309** 1–7

[34] Zhang H, Miller E J and Yu E T 2006 Analysis of leakage current mechanisms in schottky contacts to GaN and Al0.25Ga0.75N/GaN grown by molecular-beam epitaxy *J. Appl. Phys.* **99** 023703

[35] Wang R *et al* 2021 Reducing the reverse leakage current of AlGaN/GaN heterostructures via low-fluence neutron irradiation *J. Mater. Chem.* C **9** 3177–82

[36] Yan D, Lu H, Cao D, Chen D, Zhang R and Zheng Y 2010 On the reverse gate leakage current of AlGaN/GaN high electron mobility transistors *Appl. Phys. Lett.* **97** 153503

[37] Karmalkar S, Sathaiya D M and Shur M S 2003 Mechanism of the reverse gate leakage in AlGaN/GaN high electron mobility transistors *Appl. Phys. Lett.* **82** 3976–8

[38] Ahmed F, Choi M S, Liu X and Yoo W J 2015 Carrier transport at the metal–MoS₂ interface *Nanoscale* **7** 9222–8

[39] Shriki A, Winter R, Calahorra Y, Kauffmann Y, Ankonina G, Eizenberg M and Ritter D 2017 Formation mechanism of gold-based and gold-free ohmic contacts to AlGaN/GaN heterostructure field effect transistors *J. Appl. Phys.* **121** 065301

[40] Kim J K, Jang H W and Lee J-L 2002 Mechanism for Ohmic contact formation of Ti on n-type GaN investigated using synchrotron radiation photoemission spectroscopy *J. Appl. Phys.* **91** 9214–7

[41] Kong X, Wei K, Liu G and Liu X 2012 Role of Ti/Al relative thickness in the formation mechanism of Ti/Al/Ni/Au ohmic contacts to AlGaN/GaN heterostructures *J. Phys. Appl. Phys.* **45** 265101

[42] Bright A N, Thomas P J, Weyland M, Tricker D M, Humphreys C J and Davies R 2001 Correlation of contact resistance with microstructure for Au/Ni/Al/Ti/AlGaN/GaN ohmic contacts using transmission electron microscopy *J. Appl. Phys.* **89** 3143–50

[43] Wang L, Mohammed F M and Adesida I 2005 Dislocation-induced nonuniform interfacial reactions of Ti/Al/Mo/Au ohmic contacts on AlGaN/GaN heterostructure *Appl. Phys. Lett.* **87** 141915

[44] Ibbetson J P, Fini P T, Ness K D, DenBaars S P, Speck J S and Mishra U K 2000 Polarization effects, surface states, and the source of electrons in AlGaN/GaN heterostructure field effect transistors *Appl. Phys. Lett.* **77** 250–2

[45] Higashiwaki M, Chowdhury S, Swenson B L and Mishra U K 2010 Effects of oxidation on surface chemical states and barrier height of AlGaN/GaN heterostructures *Appl. Phys. Lett.* **97** 222104

[46] Fang Z-Q, Claflin B, Look D C, Green D S and Vetury R 2010 Deep traps in AlGaN/GaN heterostructures studied by deep level transient spectroscopy: effect of carbon concentration in GaN buffer layers *J. Appl. Phys.* **108** 063706

[47] Gassoumi M, Bluet J M, Chekir F, Dermoul I, Maaref H, Guillot G, Minko A, Hoel V and Gaquière C 2006 Investigation of traps in AlGaN/GaN HEMTs by current transient spectroscopy *Mater. Sci. Eng.* C **26** 383–6

[48] Schroder D K 2006 *Semiconductor Material and Device Characterization* (IEEE Press)

[49] Lu B, Piner E L and Palacios T 2010 Schottky-drain technology for AlGaN/GaN high-electron mobility transistors *IEEE Electron Device Lett.* **31** 302–4

[50] Bahat-Treidel E, Lossy R, Wurfl J and Trankle G 2009 AlGaN/GaN HEMT with integrated recessed schottky-drain protection diode *IEEE Electron Device Lett.* **30** 901–3

[51] Mao W, She W-B, Yang C, Zhang J-F, Zheng X-F, Wang C and Hao Y 2015 Reverse blocking characteristics and mechanisms in schottky-drain AlGaN/GaN HEMT with a drain field plate and floating field plates *Chin. Phys.* B **25** 017303

[52] Zhou C, Chen W, Piner E L and Chen K J 2010 Schottky-ohmic drain AlGaN/GaN normally off HEMT with reverse drain blocking capability *IEEE Electron Device Lett.* **31** 668–70

J. Phys. D: Appl. Phys. **58** (2025) 135117

F Adams *et al*

[53] Miura N, Nanjo T, Suita M, Oishi T, Abe Y, Ozeki T, Ishikawa H, Egawa T and Jimbo T 2004 Thermal annealing effects on Ni/Au based schottky contacts on n-GaN and AlGaN/GaN with insertion of high work function metal *Solid State Electron.* **48** 689–95

[54] Yan D, Jiao J, Ren J, Yang G and Gu X 2013 Forward current transport mechanisms in Ni/Au-AlGaN/GaN schottky diodes *J. Appl. Phys.* **114** 144511

[55] Calzolaro A, Hentschel R, Edokam I F, Sizov V, Mikolajick T and Wachowiak A 2020 Material investigations for improving stability of Au free Ta/Al-based ohmic contacts annealed at low temperature for AlGaN/GaN heterostructures *Semicond. Sci. Technol.* **35** 075011

[56] Lin Y-K, Bergsten J, Leong H, Malmros A, Chen J-T, Chen D-Y, Kordina O, Zirath H, Chang E Y and Rorsman N 2018 A versatile low-resistance ohmic contact process with ohmic recess and low-temperature annealing for GaN HEMTs *Semicond. Sci. Technol.* **33** 095019